Rev. Roum. Sci. Techn.– Électrotechn. et Énerg.
Vol. **69**, *4*, pp. 373–376, Bucarest, 2024

REAL-VALUED DAMPED SINUSOID PARAMETER ESTIMATION USING A THREE-POINT INTERPOLATED DISCRETE FOURIER TRANSFORM ALGORITHM

DANIEL BELEGA[1], DARIO PETRI[2]

Keywords: Discrete Fourier transform (DFT)-based algorithms; Parameter estimation; Real-valued damped sinusoids; Statistical and error analysis; Windowing.

This paper proposes new real-valued damped sinusoid frequency and damping factor estimators. They exploit a three-point Interpolated discrete Fourier transform (IpDFT) algorithm based on the Rife-Vincent class I (RVCI) windows and complex-valued DFT samples. The accuracies of the proposed estimators are compared with those provided by other state-of-the-art interpolated Fourier algorithms using computer simulations when pure, noisy, and noisy and harmonically distorted damped sinusoids are analyzed.

1. INTRODUCTION

Real-valued damped sinusoids are used in many application domains, such as radar, optics, mechanical spectroscopy, and power systems [1–6]. The interpolated discrete Fourier transform (IpDFT) algorithms are often used since they ensure fast and accurate estimates of damped sinusoid parameters [3–10]. These algorithms reduce the picket-fence effect due to the finite number of analyzed samples by interpolating two or more suitably selected Discrete Fourier Transform (DFT) samples of the analyzed signal [11]. Interpolating more than two DFT points enables compensation for the detrimental contribution of the fundamental image component to the estimated parameters. Signal windowing is also adopted to reduce the contribution of the image component's spectral interference and other spurious tones [12–15]. The Rife-Vincent class I (RVCI) windows are often employed since they provide straightforward interpolation expressions [10,16]. These windows are also called maximum sidelobe decay (MSD) since they exhibit the highest sidelobe decay rate among all cosine windows with a given number of terms [13], thus ensuring optimal long-range spectral leakage reduction.

In [6], a three-point IpDFT algorithm for real-valued damped sinusoid parameter estimation has been proposed. It is based on the *H*-order RVCI windows, called the RVCI–H algorithm, as shown below. Frequency and damping factor estimators are obtained using two different interpolation functions based on selected DFT module samples. This paper presents a three-point IpDFT algorithm that exploits complex-valued DFT samples, which returns frequency and damping factor estimates evaluating only one interpolation function. Based on the *H*-order RVCI window, the procedure is called the Complex RVCI-H (CRVCI-H) algorithm. The accuracy of the CRVCI-H algorithm is compared with that of the RVCI-H algorithm and with those of other state-of-the-art interpolated Fourier algorithms through computer simulations considering real-valued pure, noisy, and noisy and harmonically distorted damped sinusoids.

2. THE RVCI-H AND THE CRVCI-H ALGORITHMS

The analyzed noisy discrete-time damped sinusoid is expressed as:

$$s(m) = x(m) + e(m),\ m = 0, 1, \dots, M-1. \quad (1)$$

where $x(m) = Ae^{-\frac{2\pi}{M}\alpha m}\cos\left(2\pi\frac{\nu}{M}m + \phi\right)$.

In (1) $x(\cdot)$ is the noise-free damped sinusoid of amplitude A, normalized frequency ν, phase ϕ, and normalized damping factor α, $e(\cdot)$ is an additive white Gaussian noise with zero mean and variance σ_n^2, and M is the number of acquired samples. The signal-to-noise ratio (*SNR*) of signal (1) is defined as $SNR \stackrel{\text{def}}{=} \frac{A^2}{2\sigma_n^2}$.

The signal normalized frequency can be written as:

$$\nu = l + \delta, \quad (2)$$

where l and δ ($-0.5 \le \delta < 0.5$) are the integer part and the fractional of ν, respectively, it is worth noticing that δ represents the inter-bin frequency location, which is null when coherent sampling occurs.

Signal windowing is applied to reduce the contribution of the spectral interference on the frequency and the damping factor estimates due to the image component and possible spurious tones. Thus, the analyzed signal becomes $s_w(m) = s(m) \cdot w(m)$. The adopted weighting function is the *H*-order RVCI window, defined as:

$$w(m) = \sum_{h=0}^{H}(-1)^h a_h \cos\left(\frac{2\pi hm}{M}\right), m = 0,1, \dots, M-1, \quad (3)$$

where $a_0 = \frac{C_{2H}^H}{2^{2H}}$ and $a_h = \frac{C_{2H}^{H-h}}{2^{2H-1}}, h = 1, 2, \dots, H$, with $C_p^q = \frac{p!}{(p-q)!\cdot q!}$, are the window coefficients [17].

The discrete-time Fourier transform (DTFT) of the weighted signal $s_w(\cdot)$ is given by:

$$S_w(\vartheta) = X_w(\vartheta) + E_w(\vartheta), \quad (4)$$

where $X_w(\cdot)$ and $E_w(\cdot)$ are the DTFTs of the noise free weighted damped sinusoid $x_w(m) = x(m)\cdot w(m)$ and weighted wideband noise $e_w(m) = e(m)\cdot w(m)$, respectively. $X_w(\cdot)$ can be expressed as:

$$X_w(\vartheta) = \tilde{X}_w(\vartheta) + \tilde{X}_{iw}(\vartheta), \quad (5)$$

where $\tilde{X}_w(\vartheta)$ and $\tilde{X}_{iw}(\vartheta)$ are the transforms of the fundamental component and the $x(m)$ spectral image, respectively. They are given by [10]:

$$\tilde{X}_w(\vartheta) \cong f\big(\alpha + j(\vartheta - \nu)\big)e^{j\phi}, \quad (6)$$

and

[1] Department of Measurements and Optical Electronics, University Politehnica Timișoara, Bv. V. Pârvan, 2, 3000223, Timișoara, Romania. E-mail: daniel.belega@upt.ro
[2] Department of Industrial Engineering, University of Trento, Via Sommarive, 9, 38123, Trento, Italy. E-mail: dario.petri@unitn.it

DOI: 10.59277/RRST-EE.2024.69.4.1

$$\tilde{X}_{iw}(\vartheta) \cong f\big(\alpha + j(\vartheta - \nu)\big)e^{-j\phi}, \tag{7}$$

where

$$f(z) \stackrel{\text{def}}{=} \frac{(2H)!}{2^{2H+2}} \frac{AM}{\pi} \frac{\left(1-e^{-2\pi z}\right)}{z\prod_{h=1}^{H}(z^2+h^2)}, \; z \in \mathbb{C}. \tag{8}$$

The RVCI-H algorithm estimates the inter-bin frequency location and the damping factor by using the following two different interpolation functions [6]:

$$\hat{\delta} = -\frac{2H+1}{2} \frac{R_{1m}-R_{2m}}{2(H+1)R_{1m}R_{2m}-R_{1m}-R_{2m}-2H}, \tag{9}$$

and

$$\hat{\alpha} = \sqrt{\left|\frac{(\hat{\delta}+H)^2 \cdot R_{1m}(\hat{\delta}-H-1)^2}{R_{1m}-1}\right|}, \tag{10}$$

where $R_{1m} \stackrel{\text{def}}{=} \frac{|S_w(l+1)|^2}{|S_w(l)|^2}$ and $R_{2m} \stackrel{\text{def}}{=} \frac{|S_w(l-1)|^2}{|S_w(l)|^2}$.

Unlike [6], (10) considers the expression module under the square root since it may become negative due to the contribution of the spectral image component. Moreover, it is worth noticing that the estimator $\hat{\alpha}$ depends on the estimator $\hat{\delta}$, and so is its accuracy.

As shown in the Appendix, the proposed CRVCI-H algorithm uses a single interpolation function, that is:

$$h = -\frac{2H+1}{2} \frac{R_{1c}-R_{2c}}{2(H+1)R_{1c}R_{2c}-R_{1c}-R_{2c}-2H}, \tag{11}$$

where $R_{1c} \stackrel{\text{def}}{=} \frac{S_w^2(l+1)}{S_w^2(l)}$ and $R_{2c} \stackrel{\text{def}}{=} \frac{S_w^2(l-1)}{S_w^2(l)}$.

The inter-bin frequency location and the damping factor estimators are then derived from (11), simply as (see (A.5) in Appendix):

$$\tilde{\delta} = Re\{h\}, \quad \text{and} \quad \tilde{\alpha} = Im\{h\}. \tag{12}$$

Observe that (11) coincides with (9), except that complex-valued DFT samples are used instead of DFT module samples. Also, unlike the RVCI-H algorithm, the damping factor estimator $\tilde{\alpha}$ provided by the CRVCI-H algorithm, it does not depend on the estimator $\tilde{\delta}$. Therefore, its accuracy is expected to be better than that of the estimator $\hat{\alpha}$ supplied by the RVCI-H algorithm, as shown next.

3. ACCURACY COMPARISON

This section compares the RVCI-H and the CRVCI-H algorithms' accuracies using simulations considering pure, noisy, and harmonically distorted damped sinusoids. The results returned by the classical two-point IpDFT algorithm [9] and the (two-point iterative) Aboutanios algorithm [3] are also considered when noisy and noisy and harmonically distorted signals are analyzed. Two iterations are performed in the latter algorithm [3]. The simulated signal parameters are amplitude A = 1 p.u., damping factor α = 0.1, and record length M = 512 samples. When pure damped sinusoids are analyzed for each frequency value, the signal phase ϕ is linearly changed in the range [0, 2π) rad with a step of π/50 rad. The maximum absolute values of the parameter estimation error, $|\Delta\delta|_{max}$ and $|\Delta\alpha|_{max}$, are then determined. Conversely, when noisy damped sinusoids are considered, 10,000 runs are processed for each variable parameter value, and the signal phase ϕ is randomly chosen in the range [0, 2π) rad. Accuracy is then assessed using the root mean square error (*RMSE*) or the normalized *RMSE* (*NRMSE*). This latter parameter is the ratio between the estimation *RMSE* and the square root of the related asymptotic Cramér-Rao lower bound (CRLB) [18].

The simulation results obtained are presented below.

REAL-VALUED PURE DAMPED SINUSOIDS

Figure 1 shows the maximum of the absolute values of the estimation errors, $|\Delta\delta|_{max}$ (Fig. 1(a)) and $|\Delta\alpha|_{max}$ (Fig. 1(b)), returned by both the RVCI-H and the CRVCI-H algorithms as a function of the number of analyzed signal cycles ν, which varies in the range [1.5, 8) with a step of 0.1 cycles. The rectangular (H = 0) and the two-term MSD (H = 1) or Hann windows are used.

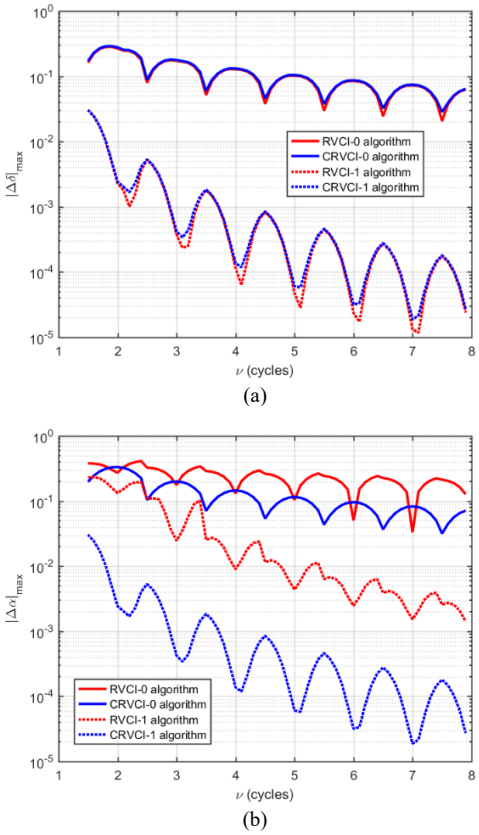

Fig. 1 – Real-valued pure damped sinusoids: maximum absolute value of the frequency $|\Delta\delta|_{max}$ (a) and the damping factor $|\Delta\alpha|_{max}$ (b) estimation errors of the RVCI-H and the CRVCI-H algorithms based on the rectangular and Hann windows versus the number of acquired signal cycles ν. M = 512 samples, signal phase ϕ linearly changed in the range [0, 2π) rad.

Figure 1 shows that the RVCI-H and the CRVCI-H algorithms are almost equally accurate when the frequency is estimated. Conversely, the CRVCI-H algorithm returns much better when assessing the damping factor. Also, low accuracy is obtained when the rectangular window is used. This occurs since that window does not significantly reduce the detrimental contribution of the spectral image component. For this reason, only the Hann window is considered in the following.

REAL-VALUED NOISY DAMPED SINUSOIDS

Figure 2 shows the *NRMSE*s of the inter-bin frequency location (Fig. 2(a)) and the damping factor (Fig. 2(b)) estimates returned by the considered algorithms as a function of the number of analyzed cycles, which varies in the range [1.5, 10) with a step of 0.1 cycles. The *SNR* is 50 dB.

As expected from the results reported in Fig. 1, the inter-bin frequency location estimates provided by the RVCI-1 and CRVCI-1 algorithms are almost equally accurate. In

contrast, the CRVCI-1 algorithm offers much more precise damping factor estimates than the RVCI-1 algorithm. Also, when ν it is smaller than about 7 cycles (situations where the contribution of the spectral image component dominates the effect of noise), the CRVCI-1 algorithm outperforms the two-point IpDFT algorithm almost everywhere. In contrast, the Aboutanios algorithm provides the most accurate estimates when $|\delta|$ is quite close to 0.5 bins. Conversely, when ν it is higher than about seven cycles (situations where the effect of noise overcomes that due to the spectral image component), all considered algorithms exhibit close accuracies, except the RVCI-1 algorithm, which provides relatively poor damping factor estimates.

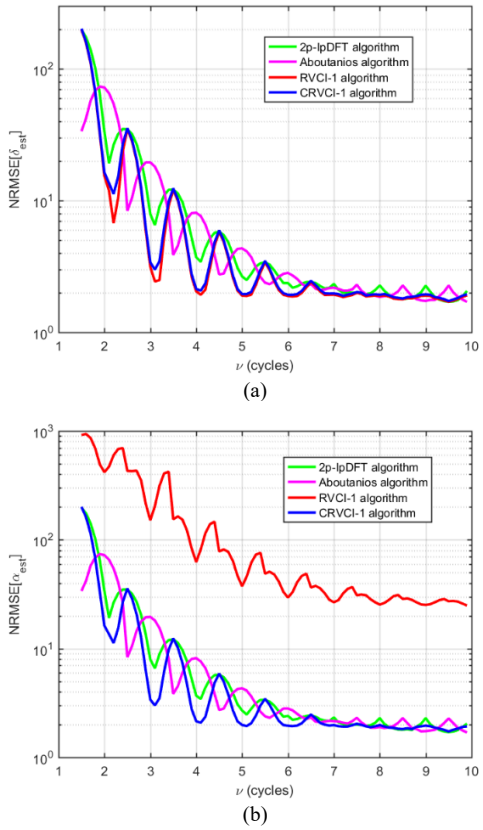

Fig. 2 – Real-valued noisy damped sinusoids: NRMSEs of the inter-bin frequency location (a) and the damping factor (b) obtained by the classical two-point IpDFT [9], the Aboutanios [3], the RVCI-1, and the CRVCI-1 algorithms versus the number of acquired signal cycles ν when SNR = 50 dB. Ten thousand runs of M = 512 samples, each with signal phase ϕ changed at random.

Figure 3 shows the RMSEs of the inter-bin frequency location (Fig. 3(a)) and the damping factor (Fig. 3(b)) estimates ensured by the considered algorithms as a function of the SNR, which varies in the range [-10, 60] dB with a step of 5 dB. The length of the observation window is ν = 3.3 cycles. In addition, the $\sqrt{\text{CRLB}}$ shown in Fig. 3 to enable a visual assessment of the algorithm's statistical efficiency.

As we can see, the RMSEs of all the considered inter-bin frequency location estimators are close as soon as the SNR is smaller than 30 dB. Conversely, the RVCI-1 and the CRVCI-1 algorithms are more accurate for higher SNR values than the others. Indeed, in this latter situation, the contribution of the spectral image component dominates the effect of noise. Still, the CRVCI-1 and the RVCI-1 are more robust to that contribution due to the adoption of three-point interpolation. A similar *RMSE* behavior holds for the damping factor estimators returned by the CRVCI-1, the two-point IpDFT, and the Aboutanios algorithms. In contrast, the RVCI-1 algorithm exhibits poor accuracy, as expected from the results reported in Fig. 2(b).

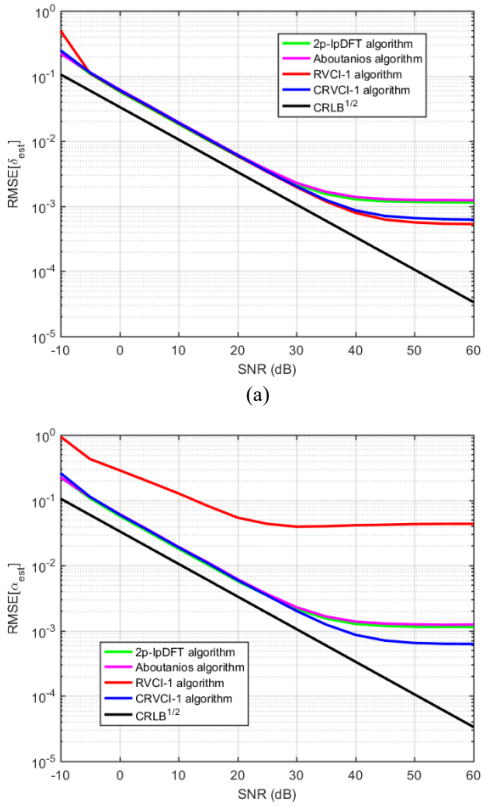

Fig. 3 – Real-valued noisy damped sinusoids: *RMSE*s of the inter-bin frequency location (a) and the damping factor (b) obtained by the classical two-point IpDFT [9], the Aboutanios [3], the RVCI-1, and the CRVCI-1 algorithms versus *SNR* when ν = 3.3 cycles. Ten thousand runs of M = 512 samples, each with signal phase ϕ changed at random.

REAL-VALUED NOISY AND HARMONICALLY DISTORTED DAMPED SINUSOIDS

Figure 4 shows the NRMSEs of the inter-bin frequency location (Fig. 4(a)) and the damping factor (Fig. 4(b)) estimates provided by the considered algorithms as function of the number of analyzed signal cycles when a noisy and harmonically distorted damped sinusoid are analyzed. The signal is affected by 2nd and 3rd damped harmonics with amplitudes equal to 10% and 5% of the fundamental amplitude and damping factors equal to 0.3 and 0.6, respectively. The SNR is 50 dB, and the observation window length varies, as in Fig. 2.

As we can see, the NRMSEs of the inter-bin frequency location estimators provided by the RVCI-1 and CRVCI-1 algorithms are pretty close and better than those of the other algorithms almost everywhere when at least three and no more than seven cycles are observed. For the remaining values ν, all algorithms provide nearly the same accuracy. The same conclusions hold for the damping factor estimates, except the RVCI-1 algorithm, which exhibits poor performance mainly because its damping factor estimates also depend on the estimated inter-bin frequency location.

Figures 2, 3, and 4 also show that, in the considered simulation conditions, the inter-bin frequency location and the damping factor estimates returned by the considered algorithms are close to the related asymptotic CRLB if the number of analyzed signal cycles is high enough that the effect of noise overcomes the contribution of the spectral image component.

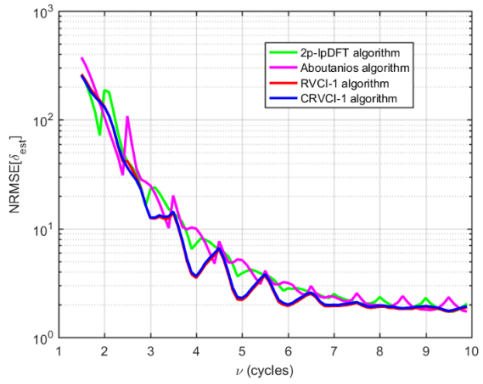

(a)

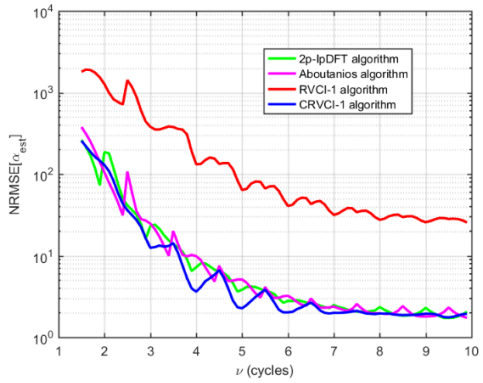

(b)

Fig. 4 – Real-valued noisy and harmonically distorted damped sinusoids: NRMSEs of the inter-bin frequency location (a) and the damping factor (b) obtained by the classical two-point IpDFT [9], the Aboutanios [3], the RVCI-1, and the CRVCI-1 algorithms versus the number of acquired signal cycles ν. Signal affected by 2nd and 3rd harmonics of amplitude 10% and 5% of the fundamental and damping factors 0.3 and 0.6, respectively. SNR = 50 dB. 10,000 runs of M = 512 samples, each with signal phase ϕ changed at random.

4. CONCLUSIONS

This paper proposes a three-point IpDFT algorithm – the CRVCI-H algorithm. It estimates the frequency and damping factor of real-valued damped sinusoids by interpolating complex-valued DFT samples, thus assuring more accurate damping factor estimates than the RVCI-H algorithm. Also, it has been shown that the CRVCI-H algorithm is more robust to the contribution of the spectral image component than the classical two-point IpDFT algorithm [9] and the Aboutanios algorithm [3]. The CRVCI-H algorithm can be advantageously employed in real-time frequency and damping factor estimation of noisy and harmonically distorted damped sinusoids.

APPENDIX

EXPRESSION OF THE INTERPOLATION FUNCTION USED BY THE CRVCI-H ALGORITHM

After simple calculations, it follows:

$$\prod_{h=1}^{H}(z^2+h^2)=\frac{(z+\mathrm{j})(z-\mathrm{j}H)}{z\big(z+\mathrm{j}(H+1)\big)}\prod_{h=1}^{H}[(z+\mathrm{j})^2+h^2]=\frac{(z-\mathrm{j})(z+\mathrm{j}H)}{z(z-\mathrm{j}(H+1))}\prod_{h=1}^{H}[(z-\mathrm{j})^2+h^2], \quad (A.1)$$

where $z = \alpha - \mathrm{j}\delta$.

By assuming that enough signal cycles are observed so that the contribution of the spectral image component to R_{1c} and R_{2c} can be neglected, after simple algebra, from (6), (8), and (A.1) it results:

$$R_{1c}\cong\frac{\tilde{X}_W^2(l+1)}{\tilde{X}_W^2(l)}\cong\frac{(z-\mathrm{j}H)^2}{\big(z+\mathrm{j}(H+1)\big)^2}, \quad (A2a)$$

and

$$R_{2c}\cong\frac{\tilde{X}_W^2(l-1)}{\tilde{X}_W^2(l)}\cong\frac{(z+\mathrm{j}H)^2}{\big(z-\mathrm{j}(H+1)\big)^2}, \quad (A.2b)$$

After tedious calculations from (A.2) it follows:

$$R_{1c}-R_{2c}\cong-\frac{4j(2H+1)z\left[z^2-H(H+1)\right]}{[z^2+(H+1)^2]^2}, \quad (A.3)$$

and

$$2(H+1)R_{1c}R_{2c}-R_{1c}-R_{2c}-2H\cong\frac{2(2H+1)^2[z^2-H(H+1)]}{[z^2+(H+1)^2]^2}. \quad (A.3)$$

By replacing (A.3) and (A.4) with (11) it follows that:

$$h\cong\delta+\mathrm{j}\alpha. \quad (A.5)$$

Received on 11 March 2024

REFERENCES

1. J.C. Visschers, E. Wilson, T. Connelly, A. Mudrov, L. Bougasi, *Rapid parameter determination of discrete damped sinusoidal oscillations*, Optics Express, **29**, *5*, pp. 6863-6878 (2021).
2. H. Günther, *NMR spectroscopy: basic principles, concepts and applications in chemistry*, John Wiley & Sons (2013).
3. E. Aboutanios, *Estimation of the frequency and decay factor of a decaying exponential in noise*, IEEE Trans. Signal Process., **58**, *2*, pp. 501–509 (2010).
4. E. Aboutanios, *Estimating the parameters of sinusoids and decaying sinusoids in noise*, IEEE Instrum. Meas. Mag., **14**, *2*, pp. 8–14 (2011).
5. D. Agrež, *Estimation of parameters of the weakly damped sinusoidal signals in the frequency domain*, Computer, Standards & Interfaces**, 33**, pp. 117-121 (2011).
6. K. Duda, T.P. Zielinski, L.B. Magalas, M. Majewski, *DFT based estimation of damped oscillation's parameters in low frequency mechanical spectroscopy*, IEEE Trans. Instrum. Meas., **60**, *11*, 2011, pp. 3608–3618 (2011).
7. M. Bertocco, C. Offeli, D. Petri, *Analysis of damped sinusoidal signals via a frequency-domain interpolation algorithm*, IEEE Trans. Instrum. Meas., **43**, *2,* pp. 245–250 (1994).
8. K. Wang, H. Wen, L. Xu, L.Wang, *Two points interpolated DFT algorithm for accurate estimation of Damping Factor and Frequency*, IEEE Signal Process Letter, **28**, pp. 499-502 (2021).
9. R. Diao, Q. Meng, H. Fan, *Interpolation algorithms based on Rife-Vincent window for discrete Fourier transforms of damped signals* (in Chinese), Journal of Mechanical Engineering, **51**, *4*, (2015).
10. D. Belega, D. Petri, *Fast interpolated DTFT estimators of frequency and damping factor of real-valued damped sinusoids*, Measurement, 217, (2023).
11. C. Offelli, D. Petri, *Interpolation techniques for real-time multifrequency waveform analysis*, IEEE Trans. Instrum. Meas., **39**, *1,* pp. 106-111 (1990).
12. F.J. Harris, *On the use of windows for harmonic analysis with the discrete Fourier transform*, Proceedings of the IEEE, **66**, *1*, pp. 51–83 (1978).
13. A.H. Nuttall, *Some windows with very good sidelobe behavior*, IEEE Trans. Acoust. Speech Signal Process. ASSP, **29**, *1* pp.84–91 (1981).
14. D.C. Rife, G.A. Vincent, *Use of the discrete Fourier transform in the measurement of frequencies and levels of tones*, Bell Syst. Tech. J, **49**, pp. 197-228 (1970).
15. D. Belega, D. Petri, D. Dallet, *Impact of harmonics on the interpolated DFT frequency estimator*, Mechanical Systems and Signal Processing, **66-67**, pp. 349-360 (2016).
16. D. Belega, D. Petri, *Effect of noise and harmonics on sine-wave frequency estimation by interpolated DFT algorithms based on few observed cycles*, Signal Processing, **140**, pp. 207-218 (2017).
17. D. Belega, D. Dallet, *Multifrequency signal analysis by interpolated DFT method with maximum sidelobe decay windows*, Measurement**, 42**, *3*, pp. 42 0-426 (2009).
18. Y. Yao, S.M. Pandit, *Cramér-Rao lower bounds for a damped sinusoidal process*, IEEE Trans. Signal Process., **43**, *4*, pp. 878–885 (1995).